2016

Magnetic resonance imaging in lung: a review of its potential for radiotherapy

Shivani Kumar
Cancer Therapy Centre Liverpool Hospital

Gary P. Liney
University of Wollongong, garyl@uow.edu.au

Robba Rai
Cancer Therapy Centre Liverpool Hospital

Lois C. Holloway
University of Wollongong, loish@uow.edu.au

Daniel Moses
University of New South Wales

See next page for additional authors

Magnetic resonance imaging in lung: a review of its potential for radiotherapy

Abstract

MRI has superior soft-tissue definition compared with existing imaging modalities in radiation oncology; this has the added benefit of functional as well as anatomical imaging. This review aimed to evaluate the current use of MRI for lung cancer and identify the potential of a MRI protocol for lung radiotherapy (RT). 30 relevant studies were identified. Improvements in MRI technology have overcome some of the initial limitations of utilizing MRI for lung imaging. A number of commercially available and novel sequences have shown image quality to be adequate for the detection of pulmonary nodules with the potential for tumour delineation. Quantifying tumour motion is also feasible and may be more representative than that seen on four-dimensional CT. Functional MRI sequences have shown correlation with flu-deoxy-glucose positron emission tomography (FDG-PET) in identifying malignant involvement and treatment response. MRI can also be used as a measure of pulmonary function. While there are some limitations for the adoption of MRI in RT-planning process for lung cancer, MRI has shown the potential to compete with both CT and PET for tumour delineation and motion definition, with the added benefit of functional information. MRI is well placed to become a significant imaging modality in RT for lung cancer.

Publication Details

Kumar, S., Liney, G., Rai, R., Holloway, L., Moses, D. & Vinod, S. K. (2016). Magnetic resonance imaging in lung: a review of its potential for radiotherapy. British Journal of Radiology, 89 (1060), 1-14.

Authors

Shivani Kumar, Gary P. Liney, Robba Rai, Lois C. Holloway, Daniel Moses, and Shalini K. Vinod

BJR

Received: 27 May 2015 | Revised: 21 January 2016 | Accepted: 1 February 2016

doi: 10.1259/bjr.20150431

Cite this article as:
Kumar S, Liney G, Rai R, Holloway L, Moses D, Vinod SK. Magnetic resonance imaging in lung: a review of its potential for radiotherapy. *Br J Radiol* 2016; **89**: 20150431.

REVIEW ARTICLE

Magnetic resonance imaging in lung: a review of its potential for radiotherapy

[1,2,3]SHIVANI KUMAR, MPH, B App Sc (MRS), [1,2,3,4]GARY LINEY, PhD, [2,3]ROBBA RAI, MHlthSc (MRI), [1,2,3,4,5]LOIS HOLLOWAY, PhD, [1,6,7]DANIEL MOSES, MEngSc, FRANZCR and [1,2,7]SHALINI K VINOD, MD, FRANZCR

[1]South Western Clinical School, School of Medicine, University of New South Wales, Liverpool, NSW, Australia
[2]Liverpool and Macarthur Cancer Therapy Centres, Liverpool Hospital, Liverpool, NSW, Australia
[3]Ingham Institute of Applied Medical Research, Liverpool, NSW, Australia
[4]Centre for Medical Radiation Physics, University of Wollongong, Liverpool, NSW, Australia
[5]Institute of Medical Physics, School of Physics, University of Sydney, Sydney, NSW, Australia
[6]Department of Medical Imaging, Northern Hospital Network, Sydney, NSW, Australia
[7]Western Sydney University, Penrith, NSW, Australia

Address correspondence to: Mrs Shivani Kumar
E-mail: *shivani.kumar@sswahs.nsw.gov.au*

ABSTRACT

MRI has superior soft-tissue definition compared with existing imaging modalities in radiation oncology; this has the added benefit of functional as well as anatomical imaging. This review aimed to evaluate the current use of MRI for lung cancer and identify the potential of a MRI protocol for lung radiotherapy (RT). 30 relevant studies were identified. Improvements in MRI technology have overcome some of the initial limitations of utilizing MRI for lung imaging. A number of commercially available and novel sequences have shown image quality to be adequate for the detection of pulmonary nodules with the potential for tumour delineation. Quantifying tumour motion is also feasible and may be more representative than that seen on four-dimensional CT. Functional MRI sequences have shown correlation with flu-deoxy-glucose positron emission tomography (FDG-PET) in identifying malignant involvement and treatment response. MRI can also be used as a measure of pulmonary function. While there are some limitations for the adoption of MRI in RT-planning process for lung cancer, MRI has shown the potential to compete with both CT and PET for tumour delineation and motion definition, with the added benefit of functional information. MRI is well placed to become a significant imaging modality in RT for lung cancer.

INTRODUCTION

Radiotherapy (RT) plays a significant role in the treatment of lung cancer[1] and relies on accurate imaging for precise treatment delivery. Improvements in imaging and the use of multimodality imaging have improved tumour delineation for RT planning and treatment of lung cancer.[2,3]

CT is the standard imaging modality in RT with a relatively high spatial resolution, but limited specificity. Tumour definition on CT can be obscured in the presence of adjacent lung collapse or consolidation. The incorporation of positron emission tomography (PET) with glucose analogue flu-deoxy-glucose (FDG) tracer has significantly improved the discrimination between benign and malignant tissue.[4] The use of FDG-PET has reduced gross tumour volumes (GTV) owing to the improved differentiation between benign and malignant tissue[5–7] and reduced interobserver variability in the delineation of GTV.[4–13] While FDG-PET with CT is currently the standard of care for tumour delineation, there are limitations. The spatial resolution of PET is poor, ranging between 5 and 7 mm compared with 2 mm for CT.[14] This low spatial resolution results in blurred edges, and tumours <4 mm may be falsely negative on FDG-PET scans. There is also a lack of consensus on the FDG-PET visualization method within RT, with a number of different methods reported in the literature.[6–9,13,15] Use of ionizing radiation to acquire images for PET and CT can be a limiting factor in repeated examinations.

The mobility of tumour and normal anatomy during respiration can lead to a large degree of uncertainty in tumour position. In order to visualize and quantify tumour motion, a number of options have been utilized including fluoroscopy, slow CT scans and breath-hold devices.[16] However, these have largely been superseded by respiratory-correlated CT or four-dimensional CT (4DCT).[17] 4DCT image acquisition is based on acquiring CT images with an external respiratory trace while the

Figure 1. Comparison of 3-T axial T_1 weighted breath-hold at inspiration gradient-echo sequence (volumetric interpolated breath-hold) (a) and T_2 weighted turbo spin-echo navigator sequence (half-Fourier acquisition single-shot turbo spin echo) at the exhale phase (b). The image in (b) demonstrates tumour infiltration into the mediastinum abutting the superior aspect of the aortic arch.

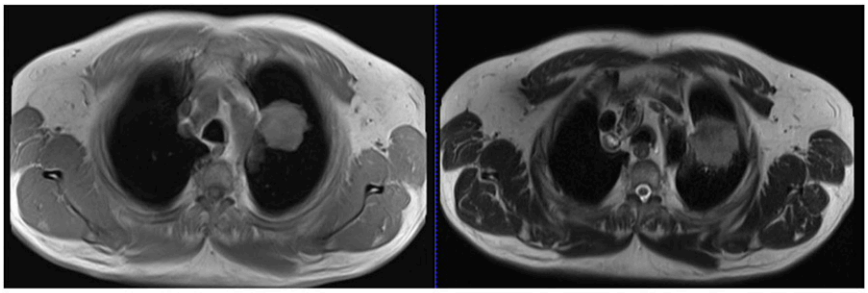

patient is free breathing. During post processing, the acquired images are correlated with an external respiratory signal usually either in the form of a reflective marker and camera system or a pressure-sensing belt around the abdomen. The advent of 4DCT in RT planning has overcome some of the problems associated with imaging the thorax[18] and has allowed for the definition of patient-specific margins for tumour motion.[19–21] However, accurate definition of motion on 4DCT is reliant on a consistent respiratory cycle.[22]

MRI is a well-established diagnostic tool in oncology.[23] Unlike CT where tissue contrast primarily depends on electron density, MRI contrast can be varied extensively by imaging other intrinsic properties of the tissue (*e.g.* spin lattice and spin–spin relaxation time, proton density, diffusion etc.). Typically, a MRI examination will consist of multiple series of scans in several imaging planes using different pulse sequences which exploit these properties.[24] This allows flexibility in facilitating optimal tumour visualization and evaluation.[23] The benefit of MRI in delineating soft tissues has been demonstrated for a number of disease sites in RT[23,25,26] and is being incorporated into the treatment-delivery process with the development of MRI linear accelerators,[27–29] making it a significant imaging modality in future. The use of MRI in the lung has been complicated by firstly by respiratory motion and also low proton density of the lung tissue, which can reduce the signal-to-noise ratio and increase magnetic susceptibility effects.[30]

Improvements in technology (most notably parallel imaging) resulting in faster acquisition times and better respiratory-gating techniques (*e.g.* navigator echoes) have significantly improved the quality of lung MRI.[31,32] Development of any MRI protocol for the lung needs minimization of the impact of susceptibility and motion artefacts on the image quality. A lung protocol for diagnostic imaging has been described[31,33] and it consists of a combination of T_2 and T_1 weighted images (Figure 1). T_2 weighted images highlight tumour infiltration and nodular lesions or masses with high fluid content, and T_1 weighted images cover high-signal pulmonary nodules and masses. For the detection of mediastinal lymph nodes, a T_2 weighted scan with fat saturation is recommended. A healthy lung generally has low signal intensity on MRI, and the presence of nodules or masses with increased proton density improves signal and contrast with the surrounding lung and therefore potential detection.[33,34]

OBJECTIVE

The aim of this study was to review the current status and developments in lung MRI in order to evaluate its potential role in: (i) target volume delineation, (ii) tumour motion quantification (iii) and functional imaging for lung cancer RT and to identify the sequences necessary to achieve these.

METHODS AND MATERIALS

A literature search was performed using PubMed, Medline and Google Scholar using the terms listed in Table 1 for articles published between 1990 and September 2014. The keyword combinations, A–H, listed in Table 1 were entered into the search strategies for each of the databases defined above to identify appropriate literature. The literature review was limited to articles written in English and on human subjects. The results were grouped according to three major areas: (1) MRI-based anatomical imaging with the potential for tumour delineation, (2) MRI-based tumour motion analysis and (3) MRI-based functional imaging.

RESULTS

30 publications were identified which met the selection criteria, 3 publications on the anatomical detection of tumour (Table 2), 9 publications on motion analysis using MRI (Table 3) and 18

Table 1. Search keywords

Keywords	Keyword combinations
(1) Lung	A: (1 and 2), (5 or 6) and (7 or 8 or 9)
(2) Cancer	B: (1 and 2) and (7 or 8 or 9)
(3) Thorax	C: (3 or 4) and (5 or 6) and (7 or 8 or 9)
(4) Thoracic	D: (3 or 4) and (7 or 8 or 9)
(5) Radiotherapy	E: (A) and (10 or 11 or 12)
(6) Radiation therapy	F: (B) and (10 or 11 or 12)
(7) MRI	G: (C) and (10 or 11 or 12)
(8) MRI	H: (D) and (10 or 11 or 12)
(9) MR	
(10) Anatomical	
(11) Motion	
(12) Functional	

Table 2. Literature summary of scan protocols for studies evaluating MRI-based anatomical detection of lung cancer

Reference	Scanner	Protocol	Acquisition plane	Breathing manoeuvre	Physiology assessed
Biederer et al[35]	1.5T (Siemens)	3D GRE VIBE	Coronal	Breath-hold 20 s	Vessels and airways
Bruegel et al[36]	1.5T (Siemens)	T_2 HASTE, T_2 IR-HASTE, T_2 TSE, STIR, VIBE	Axial	Breath-hold 14–19 s at end inspiration	Pulmonary lesions
		STIR		Respiratory and pulse triggered	
Chin et al[37]	3T (Phillips)	T_2 triple-inversion black-blood TSE, T_1 3D TSE	Axial	Breath-hold 16 s	Pulmonary nodules

3D, three-dimensional; GRE, gradient-recalled echo sequence; HASTE, half-Fourier acquisition single-shot turbo spin echo; IR-HASTE, inversion recovery HASTE; STIR, short-tau inversion recovery; TSE, turbo spin echo; VIBE, volumetric interpolated breath-hold.
GE; Milwaukee, WI; Phillips, Amsterdam, Netherlands; Siemens, Erlangen, Germany.

publications on functional MRI for lung tumour and pulmonary nodules including functional imaging of healthy lung (Table 4). The majority of the studies were conducted on 1.5-T scanners using a combination of breath-hold and free-breathing scans with and without respiratory and/or cardiac gating. Most protocols used fast-imaging-sequence variants of both the gradient-echo (GRE) or turbo-spin echo techniques. In most cases, parallel imaging—using radiofrequency coil encoding—was applied to further reduce the scan time and limit the breath-hold duration required. Table 5 highlights the basic sequences used and their applications and limitations in lung imaging. While there was evidence available for lung cancer imaging from a diagnostic perspective, there was limited evidence in its application in radiation oncology imaging.

Table 3. Literature summary of studies evaluating MRI-based tumour motion

Reference	Scanner	Protocol	Acquisition plane	Breathing manoeuvre	Physiology assessed
Biederer et al[38]	1.5T (Siemens)	3D GRE	Coronal	Phantom study	Porcine heart and lung collocated into a chest phantom
Cai et al[39]	1.5T (Siemens)	TrueFISP	Sagittal	Quiet breathing	Tumour and lung motion
Cai et al[40]	1.5T (Siemens)	TrueFISP	Sagittal	Normal breathing cycle—300-s continuous scan	Tumour and healthy lung
Koch et al[41]	1.5T (GE)	FSE fGRE	Sagittal coronal and axial	NA	Phantom
Liu et al[42]	1.5T (GE)	fGRE—modified	Axial, sagittal and coronal	Free breathing	Pulmonary vessels
Plathow et al[43]	1.5T (Siemens)	TrueFISP	Lung motion—coronal; tumour motion—sagittal, coronal	Quiet tidal breathing followed by maximum inspiration and expiration	Tumour volume, lung volume
Plathow et al[44]	1.5T (Siemens)	TrueFISP	Lung motion—coronal; tumour motion—sagittal, coronal and axial	Quiet tidal breathing followed by maximum inspiration and expiration	Lung and tumour volume
Blackall et al[45]	1.5T (Phillips)	SSFP	Coronal	Breath-hold 15 s at tidal inhalation and exhalation	Lung and tumour motion
		FFE		Free breathing	
Koch et al[46]	1.5T (GE)	fGRE—modified	Axial, sagittal and coronal	Free breathing	Pulmonary vessels

3D, three-dimensional; FFE, fast field echo; fGRE, fast gradient echo; FSE, fast spin echo; GRE, gradient echo; NA, not applicable; SSFP, steady-state free precession; TrueFISP, true fast imaging with steady-state precession.
GE; Milwaukee, WI; Phillips, Amsterdam, Netherlands; Siemens, Erlangen, Germany.

Table 4. MRI-based functional imaging

Author	Scanner	MRI protocol	b-value ($s\,mm^{-2}$)	ADC parameter	Acquisition plane	Breathing manoeuvre	Image reference	Outcome
Lichy et al[47]	1.5T (Siemens)	DWI (EPI with SE), respiratory gated	0, 400, 1000	NS	Transverse	Free breathing	FDG-PET (uptake value, NS)	Metastatic disease DWI at $b=1000\,s\,mm^{-2}$ corresponded to that on FDG-PET images; ADC maps did not improve nodal detection
Mori et al[48]	1.5T (Phillips)	DWI (EPI with SE)	1000	ADC_{min}	Transverse	Shallow breathing	FDG-PET (SUV_{max}, SUV-CR)	Inverse correlation between ADC_{min} and SUV-CR; DWI had higher sensitivity in the presence of inflammation
Pauls et al[49]	1.5 T (Siemens)	DWI (EPI with SS)	0, 400, 800	NA	Transverse	NS	FDG-PET (uptake—NS)	T_1 DCE images were equivalent to DWI in nodal detection when compared with PET; DCE and DWI understaged nodal disease when compared with PET
		DCE (T_1 2D GE+FLASH)	NA	NA	Transverse	NS		
Abdel Razek et al[50]	1.5T (Siemens)	DWI (EPI with SE)	0, 300, 600	ADC_{mean}	Transverse	NS	Histology	Mean ADC values for malignant disease significantly lower than benign nodes
Xu et al[51]	1.5T (Phillips)	DWI (EPI with SE)	0, 1000	ADC_{mean}	Transverse	Free breathing	Histology	Visual detection of malignant nodes was higher than that of benign nodes; subsequently, ADC values were significantly lower for malignant nodes when compared with benign nodes
Wang et al[52]	1.5T (Siemens)	IVIM—DWI (EPI with SS) respiratory gated	0, 5, 10, 15, 20, 25, 50, 80, 150, 300, 500, 800	NA	Transverse	Free breathing	FDG-PET histology	IVIM parameters were lower and DCE parameters were higher in the presence of disease when compared with consolidation; however, there was poor correlation between IVIM and DCE parameters
		T_1 3D VIBE	NA	NA	Transverse	Breath-hold		
Yang et al[53]	1.5T (GE)	DWI (EPI with SS SE + ASSET)	500	ADC_{mean}	Transverse	Breath-hold	FDG-PET	DWI images were equivalent to PET in the differentiation between tumour and atelectasis; T_2 images allowed differentiation between tumour and atelectasis then T_1; SCLC had higher ADC values than SCC and AC
		T_1 SE; respiratory and cardiac gated	NA	NA	Transverse	Free breathing		
		T_2 FRFSE respiratory and cardiac gated	NA	NA	Transverse	Free breathing		

(Continued)

Table 4. (Continued)

Author	Scanner	MRI protocol	b-value ($s\,mm^{-2}$)	ADC parameter	Acquisition plane	Breathing manoeuvre	Image reference	Outcome
Ohno et al[54]	3T (GE)	DWI (EPI with STIR)	1, 1000	ADC_{mean}	Transverse	Free breathing	FDG-PET (SUV_{max})	DWI (ADC) may have better potential than FDG-PET (SUV_{max}) for the prediction of tumour response during chemoradiotherapy for NSCLC
Chang et al[55]	3T (GE)	DWI (EPI with ASSET)	600	ADC_{mean}	Transverse	Breath-hold	NA	Patients who responded to treatment demonstrated increased ADC values; those who had no treatment response had a slight decrease in ADC
Yabuuchi et al[56]	1.5T (Phillips)	DWI (EPI) respiratory and pulse-gated	0, 1000	ADC_{mean}	Transverse	Free breathing	NA	Correlation between early ADC change and post-treatment tumour size; better progression-free survival in patients with increased ADC
		DCE with SE				Breath-hold		
Iizuka et al[57]	1.5T (Siemens)	DWI (EPI) respiratory gated	0, 500, 1000	ADC_{median}	Transverse	Free breathing	FDG-PET (SUV_{max})	No correlation noted between SUV_{max} and ADC_{median}; however, patients with low ADC value and high SUV_{max} demonstrated disease progression
Chen et al[58]	3T (Siemens)	DWI (EPI with SE)	50, 1000	ADC_{mean}, ADC_{median} and ADC_{min}	Transverse	Free breathing	Histology	Significant inverse relationship between tumour cellularity and ADC mean and minimum values
Hunter et al[59]	1.5T (GE)	T_1 DCE with EPI T_1 SE	NA	NA	Transverse	Quiet breathing	FDG-PET ($MRGI_c$)	Tumour vascular physiology as measured on DCE correlated with glucose metabolism; changes in vascular physiology noted during and after treatment
Regier et al[60]	1.5T (Phillips)	EPI with SE; respiratory triggered	0, 500	ADC_{min} and ADC_{mean}	Transverse	Free breathing	FDG-PET (SUV_{max} and SUV_{mean})	Inverse correlation between ADC_{min} and SUV_{max}
		T_1 3D GRE	NA	NA		Breath-hold (<20 s)		
Pauls et al[61]	1.5T (Siemens)	T_1 sGRE	NA	NA	Transverse	Maximum end inspiration breath-hold	Histology	DCE parameters allowed differentiation between tumour subtypes

(Continued)

Table 4. (Continued)

Author	Scanner	MRI protocol	b-value ($s\,mm^{-2}$)	ADC parameter	Acquisition plane	Breathing manoeuvre	Image reference	Outcome
Iwasawa et al[62]	1.5T (GE)	DCE with SE	NA	NA	Not specified	Breath-hold		DCE MRI with perfusion data allows evaluation of pulmonary perfusion
Plathow et al[63]	1.5T (Siemens)	TrueFISP	NA	NA	Coronal, sagittal and transverse	Free breathing followed by maximum inspiration and expiration	Spirometry	MRI dimensions and spirometry data demonstrated significant correlation
Shiabata et al[64]	1.5T (Philips)	bFFE	NA	NA	Mid-sagittal plane	Forced deep breathing	Spirometry	Correlation between spirometry and respiratory motion

2D, two-dimensional; 3D, three-dimensional; AC, adenocarcinoma; ADC, apparent diffusion coefficient; ADC_{mean}, mean apparent diffusion coefficient; ADC_{median}, median apparent diffusion coefficient; ADC_{min}, minimum apparent diffusion coefficient; ASSET, array spatial sensitivity encoding technique; bFFE, balanced fast-field echo; DCE, dynamic contrast-enhanced; DWI, diffusion-weighted imaging; EPI, echoplanar imaging; FLASH, fast low-angle shot; FDG, fludeoxyglucose; FRFSE, fast-recovery fast spin echo; GE, gradient echo; GRE, gradient echo; IVIM, intravoxel incoherent motion; MRGlc, glucose metabolic rate; NA, not applicable; NS, not specified; NSCLC, non-small-cell lung cancer; PET, positron emission tomography; SCC, squamous cell carcinoma; SCLC, small-cell lung cancer; SE, spin echo; sGRE, spoiled gradient echo; SS, single shot; STIR, short-tau inversion recovery; SUV, standardized uptake value; SUV-CR, contrast ratio for standardized uptake value; SUV_{max}, maximum standardized uptake value; SUV_{mean}, mean maximum standardized uptake value; TrueFISP, true fast imaging with steady-state free precision; VIBE, volumetric interpolated breath-hold.
GE, Milwaukee, WI; Phillips, Amsterdam, Netherlands; Siemens, Erlangen, Germany.

MRI-based anatomical imaging with the potential for tumour delineation

No studies specifically looked at lung tumour delineation based on MRI; however, three articles investigated the utility of MRI in detecting pulmonary nodules.[35–37] A T_1 weighted three-dimensional (3D) spoiled GRE sequence with volumetric interpolated breath-hold (VIBE) demonstrated a pulmonary nodule-detection rate comparable with CT. However, with participants who were not compliant with the breath-hold manoeuvre, blurring and ghosting artefacts impacted image quality.[35] Two studies evaluated breath-hold T_1 and T_2 weighted turbo spin-echo sequences to detect pulmonary nodules in the axial plane.[36,37] MRI was able to detect nodules between 5 and 10 mm.[37]

The main challenges for imaging in the lung are susceptibility and motion artefacts. The sequences described for pulmonary nodule detection have different applications and limitations in lung imaging. VIBE[35,36] is a 3D fast T_1 weighted spoiled GRE sequence, which is particularly robust in the presence of cardiac pulsation. With its high spatial resolution, it allows the detection of relatively small pulmonary nodules in 3D. The inherent speed of this sequence means it can be acquired in a single breath-hold.[65] It is therefore ideal in pulmonary imaging, where the entire thorax can be acquired in one breath-hold. It is, however, very sensitive to respiratory motion, which can result in significant motion-related artefacts. Being a GRE sequence, it is also prone to susceptibility artefacts especially at 3 T. T_2 weighted sequences suffer from longer acquisition times (Table 5) and therefore require gating or multiple breath-holds to be employed. To help further reduce the scan time of fast spin echoes, half-Fourier acquisition single-shot turbo spin echo has been used.[36] These sequences combine the speed-up advantages of acquiring half of the k-space data together with a single repetition time (TR) or "shot".[65.] However, this makes it prone to blurring, which may be an issue when defining the tumour volume for RT. Inversion-recovery (IR) sequences[36] with black blood contrast have also been investigated. IR protocols allow robust differentiation between the fat and water owing to the added inversion time to null the signal from the fat rather than using radiofrequency-suppression pulses. This makes it ideal for identifying the tumour and nodal volume close to the mediastinum as subcutaneous fat and bone marrow of the ribs will be saturated, allowing for greater visibility of the area of oedema and inflammation. However, it has "longer acquisition times caused by longer TRs, low signal-to-noise and tissues with similar T_1 values will all be suppressed".[66]

Miller et al[32] also highlighted the use of ultrashort echo-time (UTE) sequences to improve structural imaging. The development of UTE offers two specific advantages in lung imaging; acquiring signal at tens of microseconds minimizes susceptibility artefacts and allows image acquisition at extremely short relaxation times in lung. The resultant image provides similar contrast to that of CT. To date, this sequence has not been studied for the definition of tumour or pulmonary nodules.

MRI-based tumour motion

To capture respiratory motion during free breathing, real-time imaging is required. The majority of the studies assessing

Table 5. MRI sequence adaption for lung imaging

Sequence description	Type	Challenges for lung	Further improvements
T_2 weighted anatomy	Fast spin echo with gating (*e.g.* TSE/FSE or HASTE)	Long scan time requires gating or multiple breath-holds	Self-navigation using amplitude or phase
T_1 weighted anatomy	3D volume gradient echo (*e.g.* VIBE, LAVA) without gating	Breath-hold duration	Parallel imaging, partial k-space to reduce time of scan
Real-time motion	Steady state (*e.g.* TrueFISP, bSSFP, FIESTA)	Off-resonance and cardiac artefacts	Select appropriate FOV and use specific cardiac shim
Diffusion	Echoplanar imaging	EPI artefacts; low spatial resolution	Shaped excitation to reduce volume of the tissue
Perfusion	Dynamic fast gradient echo (*e.g.* FLASH, FSPGR) with contrast	Has to be run in one or multiple breath-holds depending on requirements	Radial k-space to reduce motion artefacts with/without motion correction

3D, three-dimensional; EPI, echoplanar imaging; FIESTA, fast imaging employing steady-state acquisition; FLASH, fast low-angle shot; FSE, fast spin echo; FSPGR, fast spoiled gradient recall echo; FOV, field of view; HASTE, half-Fourier acquisition single-shot turbo spin echo; LAVA, liver acquisition with volume acceleration; TrueFISP, true fast imaging with steady-state precession; TSE, turbo spin echo; VIBE, volumetric interpolated breath-hold.

tumour motion utilized a variation of GRE sequences.[38–44] While there is evidence to suggest that MRI data are prone to geometric distortion in the presence of motion,[30] two studies demonstrated results contrary to this.[41,45] Imaging in the sagittal and coronal planes demonstrated minimal error when compared with the axial plane using a thoracic phantom and a fast gradient-echo (fGRE) sequence.[41] The integrity of the structures was maintained on free-breathing real-time MRI scans, while a large error was noted for intracycle tidal volume reproducibility on breath-hold scans.[45]

fGRE sequences were shown to be feasible in assessing lung motion; however, pulmonary vessels rather than lung tumour were used for assessment.[42,46] Respiratory mechanics of the lung and tumour can also be assessed with a true fast imaging with steady-state precession (TrueFISP) sequence.[43,44] Plathow et al[44] demonstrated a variation in motion between tumour- and non-tumour-bearing hemithorax with the motion magnitude varying according to the tumour location. Variation in the tumour motion before and after RT was also assessed and showed no change, although there was a reduction in the craniocaudal motion of the tumour-bearing hemithorax.[43] The change in the craniocaudal motion of the tumour-bearing hemithorax was not reflected in spirometry results.

Two studies compared the motion measured on real-time MRI with that seen on 4DCT with conflicting results.[38,39] In a phantom study using GRE sequences, Bieder et al[38] showed that the lesion diameter was larger but the lesion displacement smaller on MRI than that on 4DCT. Cai et al[39] investigated the internal target volume error between real-time MRI and simulated 4DCT data. The results indicated that owing to the nature of 4DCT acquisition, the excursion of tumour motion may not be accurately depicted on a 4DCT scan. The magnitude of internal target volume error correlated with the variability in participants' breathing. Acquiring tumour motion data over a prolonged period was shown to be more accurate than limited breathing cycles.[40]

Figure 2. 3-T coronal true fast imaging with steady-state precession (TrueFISP) images without (a) and with (b) dedicated cardiac shim to minimize off-resonance artefacts.

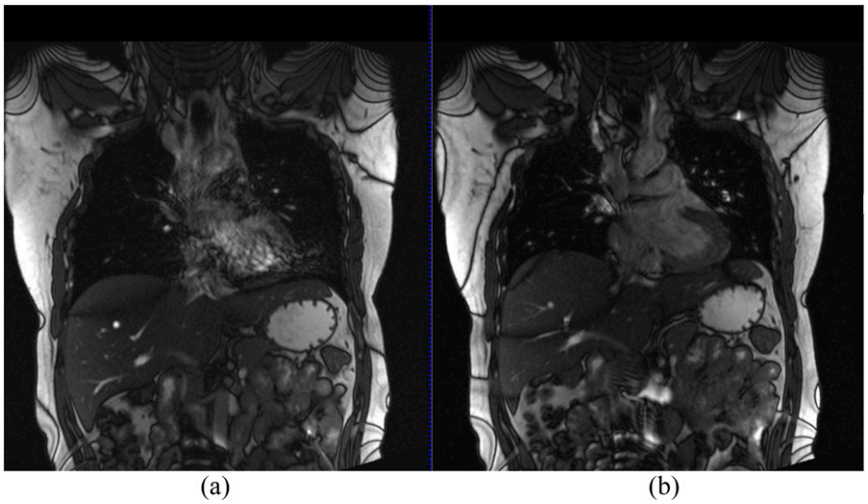

Steady-state-free precession sequences are ultrafast GREs designed around very short TRs and have demonstrated the required temporal and spatial resolution to acquire multiple images during free breathing to allow quantification of tumour motion.[65] These sequences are highly dependent on field homogeneity; it is therefore essential to perform shimming of the heart prior to acquisition to help minimize off-resonance artefacts.[65] Figure 2 demonstrates a TrueFISP sequence with and without the cardiac shim, which helps minimize artefacts. Trade-offs in temporal resolution between two-dimensional (100 ms) and 3D imaging (1 s) can lead to blurring, unless a slow-breathing manoeuvre is performed.[67]

For tumour motion assessment, an imaging protocol with ultrafast GRE sequences and parallel imaging is appropriate (Table 5). These usually consist of steady-state sequences (such as TrueFISP, steady-state free precession etc.) for optimum temporal resolution.

MRI-based functional imaging

Currently, functional imaging in lung RT satisfies two purposes, identification of nodal disease and differentiation between the tumour and surrounding consolidation. This, in most cases, is achieved with FDG-PET imaging. The most commonly employed functional MRI techniques are diffusion-weighted imaging (DWI) and dynamic contrast-enhanced (DCE) imaging. Studies looking at functional imaging included both the tumour and healthy lung tissue.

DWI is based on sensitizing the sequence to the motion of water molecules at a microscopic level (described by the b-value of the image). This motion may be quantified by generating parametric maps using at least two different b-value images and calculating the apparent diffusion coefficient (ADC). Qualitative interpretation of DWI is based on the visual assessment of signal intensity on a high b-value image set; a region of high signal intensity depicts restricted diffusion in the extracellular space. Areas of restricted diffusion will translate to areas of low values on the resulting ADC map.

A number of studies utilized DWI to assess the presence of malignant lymph nodes[47–51] and detection of tumour in the presence of consolidation.[52,53] Most studies compared DWI with FDG-PET imaging. DWI was not able to improve the detection of metastatic mediastinal nodal disease for lung cancer compared with PET;[47,48] however, it had higher specificity in the presence of inflammation.[48] Pauls et al[49] showed that DWI had 80% agreement with PET for nodal stage with 15% of the cases understaged and 5% of the cases overstaged. In those cases

Figure 3. Axial diffusion-weighted imaging (echoplanar imaging with ZOOMit) with b-value 0 (a), 250 (b), 500 (c) and 750 (d) of a 69-year-old male patient with lung cancer diagnosed with large-cell carcinoma of the left upper lobe. There is a marked area of hyperintensity in the left upper lobe characteristic of restricted diffusion. Artefacts are present, but the image quality is sufficient for tumour edge definition (d) and apparent diffusion coefficient measurement (e).

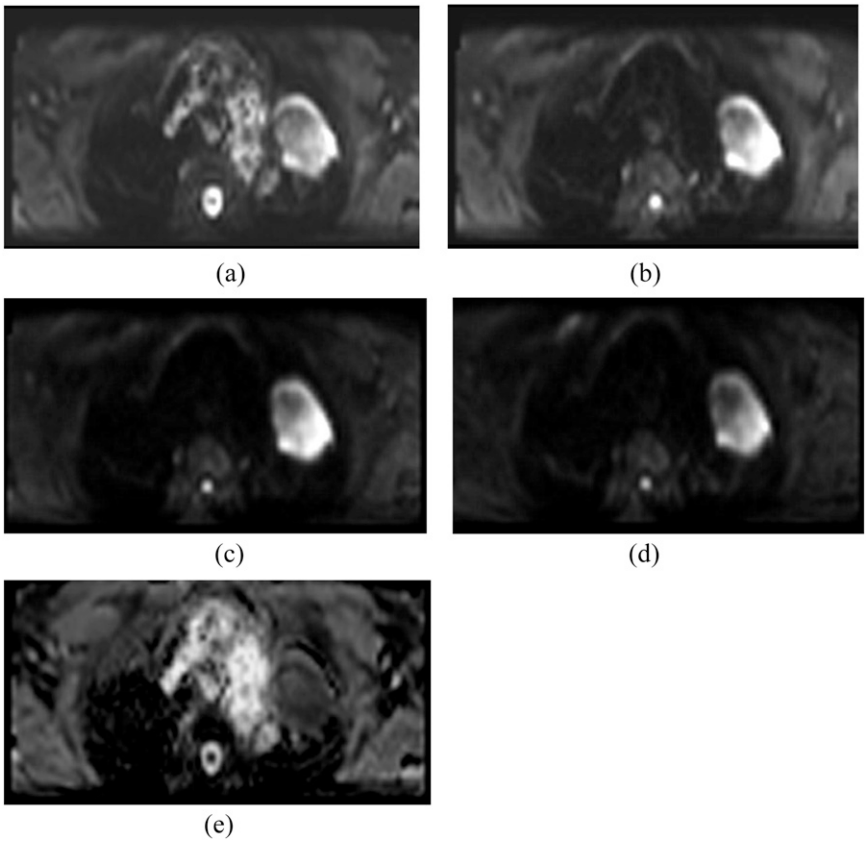

where MRI overstaged the nodal disease, restricted diffusion was noted in both mediastinal and supraclavicular lymph nodes (4–7 mm), with no evidence of elevated glucose metabolism. Nodal disease was adjacent to the primary tumour volume, in cases where MRI understaged the disease.[49] It should be noted that neither study had pathological correlation of the imaging results; both were only assessing the agreement between the two imaging modalities.[48,49] Therefore, there is potential for PET to be false negative in the case of small tumours.

DWI can also differentiate between malignant and benign mediastinal lymph nodes.[50] Malignant node detection on pre-operative DWI was compared with histologically confirmed malignant lymph node status post operatively.[51] A whole-body version of DWI termed DWIBS (diffusion-weighted imaging with background signal suppression) has been used to produce images that are visually similar to FDG-PET,[51] and the visual detection of malignant nodes on the resultant images was significantly higher for both enlarged and normal-size lymph nodes. ADC values also correlated with the visual detection rate.[51]

Two studies demonstrated the potential of DWI to differentiate lung cancer from consolidation. Yang et al[53] compared DWI with FDG-PET. DWI was able to detect the difference between tumour and consolidation in all patient cases, based on the hyperintensity of the tumour. The ADC map also demonstrated lower values in the presence of the tumour. An intravoxel incoherent motion (IVIM) sequence was also able to differentiate between tumour and consolidation as compared with both DCE and FDG-PET.[52] IVIM is a modified DWI technique in which images are acquired with lower than conventional b-values that are sensitive to blood microcirculation. Both DCE and IVIM were able to distinguish between cancer and consolidation; however, there was a poor correlation between IVIM and DCE parameters.

There is potential for the ADC map to detect early treatment-related changes better than FDG-PET.[54,55] Increase in the ADC value in the early phase of treatment correlated with final tumour size reduction, indicating potential use in detecting early treatment response.[56] Median progression-free survival in patients with increased ADC change was shown to be 12.0 months compared with 6.7 months for those patients where ADC remained stable or decreased.[56] To predict disease progression following stereotactic RT for stage I non-small-cell lung cancer, Iizuka et al[57] performed pre-treatment DWI and FDG-PET. Patients with low ADC value and higher SUV_{max} had greater disease progression, but results were not statistically significant. From a slightly different perspective, Chen et al[58] demonstrated an inverse relationship between minimum and mean ADC values and tumour cellularity.

The main application of DWI has primarily been in imaging neurological disorders. However, there is increasing evidence to utilize it in imaging for cancer detection and treatment monitoring.[68] Echoplanar imaging (EPI) sequences are commonly used for DWI but are prone to susceptibility distortion and ghosting artefacts.[65] While a breath-hold scan can be performed with EPI to eliminate motion artefact using only a single b-value, it is more common practice to acquire two or more b-values for the quantification of tumour diffusion. There is potential to improve EPI for lung DWI (Table 5) in the lung, by reducing the volume of the excited tissue and limiting artefacts from tissue outside this field of view. Figure 3 illustrates an example of DWI using EPI combined with reduced excitation.

DCE involves the acquisition of images before, during and after administration of a suitable contrast agent. Data may be evaluated and quantified in a number of ways, from simple measurements to complex pharmacokinetic modelling.[69] Highly perfused regions demonstrate a high and rapid uptake and washout of gadolinium-based contrast. DCE for perfusion assessment of lung cancer requires high temporal resolution in order to adequately assess the enhancement of the tumour volume. fGRE sequences are generally utilized with partial or shared k-space approaches to optimize temporal resolution and run with multiple short breath-hold manoeuvres over the required time course. It has recently become feasible to acquire this data during free breathing by using a radial stack of stars (Table 5), sampling scheme to compensate or even correct for motion.[70] Free-breathing perfusion data have been shown to be as reproducible as breath-hold and also better tolerated. However, further investigation is required for adaption in lung imaging.[71]

Two studies highlighted a possible relationship between metabolic activity and cellularity.[59,60] Tumour vascularity[59] on DCE and restricted diffusion[60] as measured on ADC were found to be correlated to increased FDG uptake or SUV_{max} on PET scans. Hunter et al[59] also demonstrated changes in vascular physiology which were apparent during and after treatment, highlighting the potential role in clinical management. DCE perfusion parameters can also allow identification of histological subtypes for lung cancer.[61] A number of contrast-uptake parameters were used to investigate correlation with tumour subtypes, and these played a significant role in differentiating non-small-cell lung cancer (NSCLC) from small-cell lung cancer (SCLC). Time-dependent kinetic parameters were more relevant in differentiating adenocarcinoma from squamous-cell carcinoma.

Functional MRI data can also be used to assess healthy lung function prior to the course of treatment. Iwasawa et al[62] evaluated whether functional MRI could predict post-operative lung function. A correlation was seen between the perfusion ratio on MRI and radionuclide study (scintigraphy) and also between the

Table 6. Image modality comparison table

Radiotherapy end point	Imaging modality		
	CT	PET	MRI
Tumour volume delineation	✓	×	✓[35–37]
Tumour motion assessment	✓[16–21]	×	✓[38–46]
Functional information	×	✓[4]	✓[47–63]

PET, positron emission tomography.

predicted FEV1 on MRI and the tested FEV1 post operatively. MRI can also be a useful tool in evaluating respiratory mechanics and volumetry. Using the diaphragm and chest wall motion as measured on MRI imaging, Plathow et al[63] created a volumetric model to calculate vital capacity and compared this with spirometry-based vital capacity measurement as lung function tests. They were able to show a strong correlation between the vital capacity measurement on MRI and that measured on spirometry. Similarly, Shibata et al[64] investigated the difference in respiratory motion between healthy individuals and patients with chronic obstructive pulmonary disease, tracking pulmonary vessels using an in-house developed algorithm. MRI-based respiratory motion correlated strongly with spirometry data.

While not yet in routine clinical use, MRI using hyperpolarized gases or oxygen enhancement can allow for ventilation studies of the lung.[34] For hyperpolarized imaging, two noble gases are predominantly used, 3-helium (^{3}He) and 129-xenon (^{129}Xe). ^{3}He has been used to asses ventilation in post-treatment assessment[72,73] or identifying well-ventilated lung for avoidance of functional lung at the time of treatment planning.[74,75] ^{129}Xe has the added advantage in that it can be imaged following ventilation perfusion and it has been shown to highlight gas exchange impairment.[76] Oxygen-enhanced MRI utilizes pure oxygen as the contrast agent to study ventilation abnormalities.[77]

DISCUSSION

Improvements in MRI technology continue to enable the imaging of low-proton-density lung tissue in the presence of respiratory and cardiac motion. The main challenges of lung RT are accurate identification of the GTV and nodal volume, particularly in the presence of pathological changes in the surrounding lung tissue. Accurate measurement of tumour motion is also necessary to ensure that the RT field encompasses appropriate margins. MRI has the potential to help overcome both these challenges. Table 6 highlights the potential application of MRI in the RT process of lung cancer.

However, the universal application of MRI in lung RT is currently limited by the ability to generate treatment plans on MRI data sets and create reference images for treatment verification. Currently, MRI is used for specific lung cancer cases (*e.g.* Pancoast tumours) to aid in anatomical delineation; however, the CT data set is still used for treatment planning. The image registration process between CT and MRI is prone to error owing to changes in the position and shape of the organ and tumour, even if the scans are contemporaneous. A MRI-only RT workflow is being considered for many RT sites and will be necessary for MRI-guided RT systems such as the MRI linear accelerator. RT treatment-planning systems still require CT or CT-equivalent data for dose calculation. A number of methods have been proposed to derive CT equivalent data from MR images.[78] Assigning bulk density to the entire patient anatomy is the simplest solution, and has been shown to give acceptable dosimetric accuracy.[79] The previously mentioned UTE sequences may also have a role in improving bone and tissue classification and direct CT conversion approaches, which makes their application in the lung even more interesting.[79]

In addition, for lung GTV delineation, detection of a pulmonary nodule or mass is just as important as being able to define the boundary of the nodule or mass. To allow volume definition, tumour infiltration into the chest wall and or mediastinum is required along with detection of involved mediastinal lymph nodes. A combination of sequences is required to facilitate GTV delineation. T_2 weighted images such as half-Fourier acquisition single-shot turbo spin echo (HASTE) or short-tau inversion recovery (STIR) can demonstrate tumour infiltration. T_1 weighted images are ideal for identifying mediastinal lymph nodes. A limitation of these sequences for anatomical detection is that they are either breath-hold or respiratory-gated images. The exhale phase in respiratory gating with bellows or navigation is generally used, as this is the longest period of relaxation during the respiratory cycle. Knowledge regarding the deformation of tumour volume during the respiratory cycle is important. Hence, a more dynamic approach to imaging is required or at the very least anatomical scans at inspiration and expiration to capture the position and shape of the tumour at the extremes of the respiratory cycle. Imaging requirements for RT are different from those of diagnostic imaging. Imaging for RT serves the purpose of tumour and associated nodal volume delineation rather than detection and staging via diagnostic imaging. As such, these anatomical image sequences need to be further assessed in a radiation oncology setting.

There is evidence supporting the value of MRI in quantifying lung tumour motion. However, the data reported are predominantly based on sagittal and coronal planes, imaging planes that in most cases are not compatible with the majority of RT-planning systems. Furthermore, image acquisition is generally in two dimensions with either a single plane or the given number of planes through the region of interest. This can potentially neglect any out-of-plane tumour motion during respiration and introduce geometric errors in the planning process. Further study into 3D registration and incorporation of non-axial data into treatment-planning systems is needed. While 4DCT remains the gold standard for lung tumour motion, it is limited by the number of breathing cycles acquired and any irregularity in breathing. Real-time MRI can be acquired over a greater number of respiratory cycles to better understand and capture motion over time and is not influenced by irregular breathing patterns as 4DCT currently is.

In terms of functional imaging, FDG-PET remains the gold standard in defining metabolically active disease, particularly in mediastinal nodes and in the presence of consolidation. There is evidence to support DWI with ADC mapping and DCE MRI as an alternative to FDG-PET for assessing functional tumour activity. However, studies to date have all been from a diagnostic perspective, where the end points are disease presence or absence. For RT, the definition of the malignant target volume is necessary. Further research is needed to determine whether MRI will be a complementary or competing technology for PET imaging in the lung. The availability of hybrid PET-MR systems also offers promise for lung imaging.[80]

While the use of ADC and DWI imaging has been reported on extensively for lung cancer, it should be noted that

reproducibility of quoted ADC parameters such as the minimum, maximum and mean is a consideration. Kivrak et al[81] demonstrated this in their study of ADC values across six different MRI scanners with a phantom. However, rather than looking at ADC values, the analysis of histogram distributions[81] shows potential and may be better for comparing data acquired on different scanners.[82] Conversely, DWI is reproducible between scanners and has shown good interobserver and intraobserver agreement for lung cancer for tumour sizes >2 cm.[83] The ability to differentiate histological subtypes is potentially useful for patients in whom biopsy confirmation of lung cancer is not possible, usually owing to underlying lung disease. Histological subtype is important in determining treatment, and MRI parameters could have a potential role in this.[61]

However, improvement in the standard EPI technique is required to overcome some of the current limitations of susceptibility and motion artefacts.

Fundamentally, breath-hold MRI scans are challenging for patients with lung cancer owing to their already limited respiratory function. Further improvements in image technology and navigation for gating may make breath-hold scans obsolete in these patients.

Lung function tests prior to the start of any treatment to some extent dictate whether a patient is able to receive radical or palliative RT. This is usually based on spirometry to assess lung function. However, two studies[63,64] highlighted the potential of MRI to predict lung function in patients, which could be useful in patients who cannot undergo spirometry. Hyperpolarized gas- and oxygen-enhanced MRI can potentially allow for the analysis of lung microstructure and quantify ventilation and perfusion of the lung. MRI scans can thus provide an anatomical and functional representation of pulmonary function, which could potentially be used in RT planning by avoiding areas of a well-functioning lung and assessing treatment response. However, both techniques are currently restricted to research settings with limited clinical use.

MRI shows potential for monitoring of early response during a course of treatment, information which is currently not utilized in RT. There is evidence in the literature to suggest a link between early changes as seen on functional MRI and progression-free survival.[56] This information can be used to adapt treatment to an individual patient's tumour response.

CONCLUSION

Using a combination of free breathing, breath-hold and gated scans with parallel imaging techniques, the quality of lung imaging has improved, with minimal artefacts from respiratory and cardiac motion. There are still challenges in adopting MRI for RT imaging but nevertheless based on the evidence available in the literature, a potential lung RT-imaging protocol can include for GTV delineation a T_1 and T_2 weighted gradient and spin-echo sequence either as breath-hold or respiratory gated. Motion assessment is feasible; however, the incorporation of the motion data to RT planning needs further investigation. DWI can prove to be an ideal non-invasive imaging technique to assess functional information and assist in GTV delineation. A DCE scan has the potential to provide additional information on the vascular nature of the tumour volume and healthy lung perfusion. However, imaging sequences need to be further assessed in the radiation oncology setting to evaluate and further develop RT-specific requirements.

REFERENCES

1. Armstrong JG. Target volume definition for three-dimensional conformal radiation therapy of lung cancer. *Br J Radiol* 1998; **71**: 587–94. doi: http://dx.doi.org/10.1259/bjr.71.846.9849380
2. Mac Manus MP, Hicks RJ. The role of positron emission tomography/computed tomography in radiation therapy planning for patients with lung cancer. *Semin Nucl Med* 2012; **42**: 308–19. doi: http://dx.doi.org/10.1053/j.semnuclmed.2012.04.003
3. Haasbeek CJA, Slotman BJ, Senan S. Radiotherapy for lung cancer: Clinical impact of recent technical advances. *Lung Cancer* 2009; **64**: 1–8. doi: http://dx.doi.org/10.1016/j.lungcan.2008.07.008
4. Caldwell CB, Mah K, Ung YC, Danjoux CE, Balogh JM, Ganguli SN, et al. Observer variation in contouring gross tumor volume in patients with poorly defined non-small-cell lung tumors on CT: the impact of 18FDG-hybrid PET fusion. *Int J Radiat Oncol Biol Phys* 2001; **51**: 923–31. doi: http://dx.doi.org/10.1016/S0360-3016(01)01722-9
5. Ashamalla H, Rafla S, Parikh K, Mokhtar B, Goswami G, Kambam S, et al. The contribution of integrated PET/CT to the evolving definition of treatment volumes in radiation treatment planning in lung cancer. *Int J Radiat Oncol Biol Phys* 2005; **63**: 1016–23. doi: http://dx.doi.org/10.1016/j.ijrobp.2005.04.021
6. Bradley J, Thorstad WL, Mutic S, Miller TR, Dehdashti F, Siegel BA, et al. Impact of FDG-PET on radiation therapy volume delineation in non-small-cell lung cancer. *Int J Radiat Oncol Biol Phys* 2004; **59**: 78–86. doi: http://dx.doi.org/10.1016/j.ijrobp.2003.10.044
7. Spratt DE, Diaz R, McElmurray J, Csiki I, Duggan D, Lu B, et al. Impact of FDG PET/CT on delineation of the gross tumor volume for radiation planning in non-small-cell lung cancer. *Clin Nucl Med* 2010; **35**: 237–43. doi: http://dx.doi.org/10.1097/RLU.0b013e3181d18eb0
8. Fox JL, Rengan R, O'Meara W, Yorke E, Erdi Y, Nehmeh S, et al. Does registration of PET and planning CT images decrease interobserver and intraobserver variation in delineating tumor volumes for non-small-cell lung cancer? *Int J Radiat Oncol Biol Phys* 2005; **62**: 70–5. doi: http://dx.doi.org/10.1016/j.ijrobp.2004.09.020
9. Deniaud-Alexandre E, Touboul E, Lerouge D, Grahek D, Foulquier JN, Petegnief Y, et al. Impact of computed tomography and 18F-deoxyglucose coincidence detection emission tomography image fusion for optimization of conformal radiotherapy in non-small-cell lung cancer. *Int J Radiat Oncol Biol Phys* 2005; **63**: 1432–41. doi: http://dx.doi.org/10.1016/j.ijrobp.2005.05.016
10. MacManus M, Nestle U, Rosenzweig KE, Carrio I, Messa C, Belohlavek O, et al. Use of PET and PET/CT for radiation therapy planning: IAEA expert report 2006–2007. *Radiother Oncol* 2009; **91**: 85–94. doi:

http://dx.doi.org/10.1016/j.radonc.2008.11.008
11. Nestle U, Walter K, Schmidt S, Licht N, Nieder C, Motaref B, et al. 18 F-Deoxyglucose positron emission tomography (FDG-PET) for the planning of radiotherapy in lung cancer: high impact in patients with atelectasis. *Int J Radiat Oncol Biol Phys* 1999; **44**: 593–7. doi: http://dx.doi.org/10.1016/S0360-3016(99)00061-9
12. Senan S, De Ruysscher D. Critical review of PET-CT for radiotherapy planning in lung cancer. *Crit Rev Oncol Hematol* 2005; **56**: 345–51. doi: http://dx.doi.org/10.1016/j.critrevonc.2005.05.001
13. Steenbakkers RJ, Duppen JC, Fitton I, Deurloo KE, Zijp LJ, Comans EFI, et al. Reduction of observer variation using matched CT-PET for lung cancer delineation: a three-dimensional analysis. *Int J Radiat Oncol Biol Phys* 2006; **64**: 435–48. doi: http://dx.doi.org/10.1016/j.ijrobp.2005.06.034
14. De Ruysscher D, Belderbos J, Reymen B, van Elmpt W, van Baardwijk A, Wanders R, et al. State of the art radiation therapy for lung cancer 2012: a glimpse of the future. *Clin Lung Cancer* 2013; **14**: 89–95. doi: http://dx.doi.org/10.1016/j.cllc.2012.06.006
15. Nestle U, Kremp S, Schaefer-Schuler A, Sebastian-Welsch C, Hellwig D, Rube C, et al. Comparison of different methods for delineation of ^{18}F-FDG PET-Positive tissue for target volume definition in radiotherapy of patients with non-small cell lung cancer. *J Nucl Med* 2005; **46**: 1342–8.
16. Keall PJ, Mageras GS, Balter JM, Emery RS, Forster KM, Jiang SB, et al. The management of respiratory motion in radiation oncology report of AAPM Task Group 76. *Med Phys* 2006; **33**: 3874–900. doi: http://dx.doi.org/10.1118/1.2349696
17. Ford E, Mageras G, Yorke E, Ling C. Respiration-correlated spiral CT: a method of measuring respiratory-induced anatomic motion for radiation treatment planning. *Med Phys* 2003; **30**: 88. doi: http://dx.doi.org/10.1118/1.1531177
18. Balter JM, Ten Haken RK, Lawrence TS, Lam KL, Robertson JM. Uncertainties in CT-based radiation therapy treatment planning associated with patient breathing. *Int J Radiat Oncol Biol Phys* 1996; **36**: 167–74. doi: http://dx.doi.org/10.1016/S0360-3016(96)00275-1
19. Keall P. 4-dimensional computed tomography imaging and treatment planning. *Semin Radiat Oncol* 2004; **14**: 81–90. doi: http://dx.doi.org/10.1053/j.semradonc.2003.10.006
20. Rietzel E, Liu AK, Doppke KP, Wolfgang JA, Chen AB, Chen GT, et al. Design of 4D treatment planning target volumes. *Int J Radiat Oncol Biol Phys* 2006; **66**: 287–95. doi: http://dx.doi.org/10.1016/j.ijrobp.2006.05.024
21. Starkschall G, Britton K, McAleer MF, Jeter MD, Kaus MR, Bzdusek K, et al. Potential dosimetric benefits of four-dimensional radiation treatment planning. *Int J Radiat Oncol Biol Phys* 2009; **73**: 1560–5. doi: http://dx.doi.org/10.1016/j.ijrobp.2008.12.024
22. Sarker J, Chu A, Mui K, Wolfgang JA, Hirsch AE, Chen GT, et al. Variations in tumor size and position due to irregular breathing in 4D-CT: a simulation study. *Med Phys* 2010; **37**: 1254. doi: http://dx.doi.org/10.1118/1.3298007
23. Khoo VS, Joon DL. New developments in MRI for target volume delineation in radiotherapy.. *Br J Radiol* 2006; **79**: Spec-15. doi: http://dx.doi.org/10.1259/bjr/41321492
24. Khoo VS, Dearnaley DP, Finnigan DJ, Padhani A, Tanner SF, Leach MO. Magnetic resonance imaging (MRI): considerations and applications in radiotherapy treatment planning. *Radiother Oncol* 1997; **42**: 1–15. doi: http://dx.doi.org/10.1016/S0167-8140(96)01866-X
25. Dirix P, Haustermans K, Vandecaveye V. The value of magnetic resonance imaging for radiotherapy planning. *Semin Radiat Oncol* 2014; **24**: 151–9. doi: http://dx.doi.org/10.1016/j.semradonc.2014.02.003
26. Liney G, Holloway L. *MRI in radiotherapy.* RAD Magazine; 2013. pp. 19–20.
27. Fallone BG. The rotating biplanar linac–magnetic resonance imaging system. *Semin Radiat Oncol* 2014; **24**: 200–2. doi: http://dx.doi.org/10.1016/j.semradonc.2014.02.011
28. Keall PJ, Barton M, Crozier S. The Australian magnetic resonance imaging–linac program. *Semin Radiat Oncol* 2014; **24**: 203–6. doi: http://dx.doi.org/10.1016/j.semradonc.2014.02.015
29. Lagendijk JJ, Raaymakers BW, van Vulpen M. The magnetic resonance imaging–linac system. *Semin Radiat Oncol* 2014;; **24**: 207–9. doi: http://dx.doi.org/10.1016/j.semradonc.2014.02.009
30. Wild J, Marshall H, Bock M, Schad L, Jakob P, Puderbach M, et al. MRI of the lung (1/3): methods. *Insights Imaging* 2012; **3**: 345–53. doi: http://dx.doi.org/10.1007/s13244-012-0176-x
31. Biederer J, Mirsadraee S, Beer M, Molinari F, Hintze C, Bauman G, et al. MRI of the lung (3/3)—current applications and future perspectives. *Insights Imaging* 2012; **3**: 373–86. doi: http://dx.doi.org/10.1007/s13244-011-0142-z
32. Miller GW, Mugler JP, Sá RC, Altes TA, Prisk GK, Hopkins SR. Advances in functional and structural imaging of the human lung using proton MRI. *NMR Biomed* 2014; **27**: 1542–56. doi: http://dx.doi.org/10.1002/nbm.3156
33. Biederer J, Beer M, Hirsch W, Wild J, Fabel M, Puderbach M, et al. MRI of the lung (2/3). Why… when… how? *Insights Into Imaging* 2012; **3**: 373–86. doi: http://dx.doi.org/10.1007/s13244-011-0142-z
34. Wielpütz M, Kauczor HU. MRI of the lung: state of the art. *Diagn Interv Radiol* 2012; **18**: 344–53. doi: http://dx.doi.org/10.4261/1305-3825.DIR.5365-11.0
35. Biederer J, Both M, Graessner J, Liess C, Jakob P, Reuter M, et al. Lung morphology: fast MR imaging assessment with a volumetric interpolated breath-hold technique: initial experience with patients. *Radiology* 2003; **226**: 242–9. doi: http://dx.doi.org/10.1148/radiol.2261011974
36. Bruegel M, Gaa J, Woertler K, Ganter C, Waldt S, Hillerer C, et al. MRI of the lung: value of different turbo spin-echo, single-shot turbo spin-echo, and 3D gradient-echo pulse sequences for the detection of pulmonary metastases. *J Magn Reson Imaging* 2007; **25**: 73–81. doi: http://dx.doi.org/10.1002/jmri.20824
37. Chin AY, Jeon TY, Lee KS, Lee JH, Seo JB, Kim YK, et al. 3-T MRI: usefulness for evaluating primary lung cancer and small nodules in lobes not containing primary tumors. *AJR Am J Roentgenol* 2007; **189**: 386–92.
38. Biederer J, Hintze C, Fabel M, Dinkel J. Magnetic resonance imaging and computed tomography of respiratory mechanics. *J Magn Reson Imaging* 2010; **32**: 1388–97. doi: http://dx.doi.org/10.1002/jmri.22386
39. Cai J, Read PW, Baisden JM, Larner JM, Benedict SH, Sheng K. Estimation of error in maximal intensity projection-based internal target volume of lung tumors: a simulation and comparison study using dynamic magnetic resonance imaging. *Int J Radiat Oncol Biol Phys* 2007; **69**: 895–902. doi: http://dx.doi.org/10.1016/j.ijrobp.2007.07.2322
40. Cai J, Read PW, Larner JM, Jones DR, Benedict SH, Sheng K. Reproducibility of interfraction lung motion probability distribution function using dynamic MRI: statistical analysis. *Int J Radiat Oncol Biol Phys* 2008; **72**: 1228–35. doi: http://dx.doi.org/10.1016/j.ijrobp.2008.07.028
41. Koch N, Liu HH, Olsson LE, Jackson EF. Assessment of geometrical accuracy of magnetic resonance images for radiation therapy of lung cancers. *J Appl Clin Med Phys* 2003; **4**: 352–64. doi: http://dx.doi.org/10.1120/1.1617211
42. Liu HH, Koch N, Starkschall G, Jacobson M, Forster K, Liao Z, et al. Evaluation of internal

lung motion for respiratory-gated radiotherapy using MRI: Part II - Margin reduction of internal target volume. *Int J Radiat Oncol Biol Phys* 2004; **60**: 1473–83. doi: http://dx.doi.org/10.1016/j.ijrobp.2004.05.054
43. Plathow C, Hof H, Kuhn S, Puderbach M, Ley S, Biederer J, et al. Therapy monitoring using dynamic MRI: analysis of lung motion and intrathoracic tumor mobility before and after radiotherapy. *Eur Radiol* 2006; **16**: 1942–50. doi: http://dx.doi.org/10.1007/s00330-006-0237-y
44. Plathow C, Ley S, Fink C, Puderbach M, Hosch W, Schmahl A, et al. Analysis of intrathoracic tumor mobility during whole breathing cycle by dynamic MRI. *Int J Radiat Oncol Biol Phys* 2004; **59**: 952–9. doi: http://dx.doi.org/10.1016/j.ijrobp.2003.12.035
45. Blackall JM, Ahmad S, Miquel ME, McClelland JR, Landau DB, Hawkes DJ. MRI-based measurements of respiratory motion variability and assessment of imaging strategies for radiotherapy planning. *Phys Med Biol* 2006; **51**: 4147–69. doi: http://dx.doi.org/10.1088/0031-9155/51/17/003
46. Koch N, Liu HH, Starkschall G, Jacobson M, Forster K, Liao Z, et al. Evaluation of internal lung motion for respiratory-gated radiotherapy using MRI: part I—correlating internal lung motion with skin fiducial motion. *Int J Radiat Oncol Biol Phys* 2004; **60**: 1459–72. doi: http://dx.doi.org/10.1016/j.ijrobp.2004.05.055
47. Lichy MPM, Aschoff PMD, Plathow CMD, Stemmer AM, Horger WM, Mueller-Horvat CMD, et al. Tumor detection by diffusion-weighted MRI and ADC-mapping—initial clinical experiences in comparison to PET-CT. *Invest Radiol* 2007; **42**: 605–13. doi: http://dx.doi.org/10.1097/RLI.0b013e31804ffd49
48. Mori T, Nomori H, Ikeda K, Kawanaka K, Shiraishi S, Katahira K, et al. Diffusion-weighted magnetic resonance imaging for diagnosing malignant pulmonary nodules/masses: comparison with positron emission tomography. *J Thorac Oncol* 2008; **3**: 358–64. doi: http://dx.doi.org/10.1097/JTO.0b013e318168d9ed
49. Pauls S, Schmidt SA, Juchems MS, Klass O, Luster M, Reske SN, et al. Diffusion-weighted MR imaging in comparison to integrated [18F]-FDG PET/CT for N-staging in patients with lung cancer. *Eur J Radiol* 2012; **81**: 178–82. doi: http://dx.doi.org/10.1016/j.ejrad.2010.09.001
50. Abdel Razek AA, Elkammary S, Elmorsy AS, Elshafey M, Elhadedy T. Characterization of mediastinal lymphadenopathy with diffusion-weighted imaging. *Magn Reson Imaging* 2011; **29**: 167–72. doi: http://dx.doi.org/10.1016/j.mri.2010.08.002
51. Xu L, Tian J, Liu Y, Li C. Accuracy of diffusion-weighted (DW) MRI with background signal suppression (MR-DWIBS) in diagnosis of mediastinal lymph node metastasis of nonsmall-cell lung cancer (NSCLC). *J Magn Reson Imaging* 2013; **40**: 200–5. doi: http://dx.doi.org/10.1002/jmri.24343
52. Wang LL, Lin J, Liu K, Chen CZ, Liu H, Lv P, et al. Intravoxel incoherent motion diffusion-weighted MR imaging in differentiation of lung cancer from obstructive lung consolidation: comparison and correlation with pharmacokinetic analysis from dynamic contrast-enhanced MR imaging. *Eur Radiol* 2014; **24**: 1914–22. doi: http://dx.doi.org/10.1007/s00330-014-3176-z
53. Yang RM, Li L, Wei XH, Guo YM, Huang YH, Lai LS, et al. Differentiation of central lung cancer from atelectasis: comparison of diffusion-weighted MRI with PET/CT. *PLoS ONE* 2013; **8**: e60279. doi: http://dx.doi.org/10.1371/journal.pone.0060279
54. Ohno Y, Koyama H, Yoshikawa T, Matsumoto K, Aoyama N, Onishi Y, et al. Diffusion-weighted MRI versus 18F-FDG PET/CT: performance as predictors of tumor treatment response and patient survival in patients with non–small cell lung cancer receiving chemoradiotherapy. *AJR Am J Roentgenol* 2012; **198**: 75–82. doi: http://dx.doi.org/10.2214/AJR.11.6525
55. Chang Q, Wu N, Ouyang H, Huang Y. Diffusion-weighted magnetic resonance imaging of lung cancer at 3.0 T: a preliminary study on monitoring diffusion changes during chemoradiation therapy. *Clin Imaging* 2012; **36**: 98–103. doi: http://dx.doi.org/10.1016/j.clinimag.2011.07.002
56. Yabuuchi H, Hatakenaka M, Takayama K, Matsuo Y, Sunami S, Kamitani T, et al. Non–small cell lung cancer: detection of early response to chemotherapy by using contrast-enhanced dynamic and diffusion-weighted MR Imaging. *Radiology* 2011; **261**: 598–604. doi: http://dx.doi.org/10.1148/radiol.11101503
57. Iizuka Y, Matsuo Y, Umeoka S, Nakamoto Y, Ueki N, Mizowaki T, et al. Prediction of clinical outcome after stereotactic body radiotherapy for non-small cell lung cancer using diffusion-weighted MRI and 18F-FDG PET. *Eur J Radiol* 2014; **83**: 2087–92. doi: http://dx.doi.org/10.1016/j.ejrad.2014.07.018
58. Chen L, Zhang J, Chen Y, Wang W, Zhou X, Yan X, et al. Relationship between apparent diffusion coefficient and tumour cellularity in lung cancer. *PLoS ONE* 2014; **9**: e99865. doi: http://dx.doi.org/10.1371/journal.pone.0099865
59. Hunter GJ, Hamberg LM, Choi N, Jain RK, McCloud T, Fischman AJ. Dynamic T1-weighted magnetic resonance imaging and positron emission tomography in patients with lung cancer: correlating vascular physiology with glucose metabolism. *Clin Cancer Res* 1998; **4**: 949–55.
60. Regier M, Derlin T, Schwarz D, Laqmani A, Henes FO, Groth M, et al. Diffusion weighted MRI and 18F-FDG PET/CT in non-small cell lung cancer (NSCLC): does the apparent diffusion coefficient (ADC) correlate with tracer uptake (SUV)? *Eur J Radiol* 2012; **81**: 2913–8. doi: http://dx.doi.org/10.1016/j.ejrad.2011.11.050
61. Pauls S, Breining T, Muche R, Schmidt SA, Wunderlich A, Kruger S, et al. The role of dynamic, contrast-enhanced MRI in differentiating lung tumor subtypes. *Clin Imaging* 2011; **35**: 259–65. doi: http://dx.doi.org/10.1016/j.clinimag.2010.07.002
62. Iwasawa T, Saito K, Ogawa N, Ishiwa N, Kurihara H. Prediction of postoperative pulmonary function using perfusion magnetic resonance imaging of the lung. *J Magn Reson Imaging* 2002; **15**: 685–92. doi: http://dx.doi.org/10.1002/jmri.10121
63. Plathow C, Ley S, Fink C, Puderbach M, Heilmann M, Zuna I, et al. Evaluation of chest motion and volumetry during the breathing cycle by dynamic MRI in healthy subjects: comparison with pulmonary function tests. *Invest Radiol* 2004; **39**: 202–9. doi: http://dx.doi.org/10.1097/01.rli.0000113795.93565.c3
64. Shibata H, Iwasawa T, Gotoh T, Kagei S, Shinohara T, Ogura T, et al. Automatic tracking of the respiratory motion of lung parenchyma on dynamic magnetic resonance imaging: comparison with pulmonary function tests in patients with chronic obstructive pulmonary disease. *J Thorac Imaging* 2011; **27**: 387–92. doi: http://dx.doi.org/10.1097/RTI.0b013e3182242b11
65. Bernstein MA, King KF, Zhou XJ. *Handbook of MRI pulse sequences*. Burlington, MA: Elsevier; 2004.
66. Hashemi R, Bradley W, Lisanti C. *MRI: the basics*. Philadelphia, PA: Lippincott Williams & Wilkins; 2004. pp. 82.
67. Tetzlaff R. Respiratory mechanics and pulmonary motion. In: Kauczor HU, editor. *MRI of the lung. Medical radiology*. Heidelberg, Berlin: Springer 2009. pp. 91–103.
68. Bozgeyik Z, Onur MR, Poyraz AK. The role of diffusion weighted magnetic resonance imaging in oncologic settings. *Quant Imaging Med Surg* 2013; **3**: 269–78. doi: http://dx.doi.org/10.3978/j.issn.2223-4292.2013.10.07
69. Henzler T, Schmid-Bindert G, Schoenberg SO, Fink C. Diffusion and perfusion MRI of

the lung and mediastinum. *Eur J Radiol* 2010; **76**: 329–36. doi: http://dx.doi.org/10.1016/j.ejrad.2010.05.005

70. Block KT, Chandarana H, Milla S, Bruno M, Mulholland T, Fatterpekar G, et al. Towards routine clinical use of radial stack-of-stars 3D gradient-echo sequences for reducing motion sensitivity. *J Korean Soc Magn Reson Med* 2014; **18**: 87–106. doi: http://dx.doi.org/10.13104/jksmrm.2014.18.2.87
71. Ingrisch M, Maxien D, Schwab F, Reiser MF, Nikolaou K, Dietrich O. Assessment of pulmonary perfusion with breath-hold and free-breathing dynamic contrast-enhanced magnetic resonance imaging: quantification and reproducibility. *Invest Radiol* 2014; **49**: 382–9. doi: http://dx.doi.org/10.1097/RLI.0000000000000020
72. Allen AM, Albert M, Caglar HB, Zygmanski P, Soto R, Killoran J, et al. Can Hyperpolarized Helium MRI add to radiation planning and follow-up in lung cancer? *J Appl Clin Med Phys* 2011; **12**: 3357.
73. Ireland RH, Din OS, Swinscoe JA, Woodhouse N, van Beek EJ, Wild JM, et al. Detection of radiation-induced lung injury in non-small cell lung cancer patients using hyperpolarized helium-3 magnetic resonance imaging. *Radiother Oncol* 2010; **97**: 244–8. doi: http://dx.doi.org/10.1016/j.radonc.2010.07.013
74. Bates EL, Bragg CM, Wild JM, Hatton MQF, Ireland RH. Functional image-based radiotherapy planning for non-small cell lung cancer: a simulation study. *Radiother Oncol* 2009; **93**: 32–6. doi: http://dx.doi.org/10.1016/j.radonc.2009.05.018
75. Ireland RH, Bragg CM, McJury M, Woodhouse N, Fichele S, Van Beek EJ, et al. Feasibility of image registration and intensity-modulated radiotherapy planning with hyperpolarized helium-3 magnetic resonance imaging for non–small-cell lung cancer. *Int J Radiat Oncol Biol Phys* 2007; **68**: 273–81. doi: http://dx.doi.org/10.1016/j.ijrobp.2006.12.068
76. Kauczor HU, Kreitner KF. Contrast-enhanced MRI of the lung. *Eur J Radiol* 2000; **34**: 196–207. doi: http://dx.doi.org/10.1016/S0720-048X(00)00199-6
77. Ohno Y, Sugimura K, Hatabu H. Clinical oxygen-enhanced magnetic resonance imaging of the lung. *Top Magn Reson Imaging* 2003; **14**: 237–43. doi: http://dx.doi.org/10.1097/00002142-200306000-00004
78. Nyholm T, Jonsson J. Counterpoint: opportunities and challenges of a magnetic resonance imaging–only radiotherapy work flow. *Semin Radiat Oncol* 2014; **24**: 175–80. doi: http://dx.doi.org/10.1016/j.semradonc.2014.02.005
79. Jonsson JH, Karlsson MG, Karlsson M, Nyholm T. Treatment planning using MRI data: an analysis of the dose calculation accuracy for different treatment regions. *Radiat Oncol* 2010; **5**: 62. doi: http://dx.doi.org/10.1186/1748-717X-5-62
80. Partovi S, Kohan A, Rubbert C, Vercher-Conejero JL, Gaeta C, Yuh R, et al. Clinical oncologic applications of PET/MRI: a new horizon. *Am J Nucl Med Mol Imaging* 2014; **4**: 202–12.
81. Kivrak AS, Paksoy Y, Erol C, Koplay M, Ozbek S, Kara F. Comparison of apparent diffusion coefficient values among different MRI platforms: a multicenter phantom study. *Diagn Interv Radiol* 2013; **19**: 433–7. doi: http://dx.doi.org/10.5152/dir.2013.13034
82. Tsien C, Cao Y, Chenevert T. Clinical applications for diffusion magnetic resonance imaging in radiotherapy. *Semin Radiat Oncol* 2014; **24**: 218–26. doi: http://dx.doi.org/10.1016/j.semradonc.2014.02.004
83. Bernardin L, Douglas N, Collins D, Giles S, O'Flynn E, Orton M. Diffusion-weighted magnetic resonance imaging for assessment of lung lesions: repeatability of the apparent diffusion coefficient measurement. *Eur Radiology* 2014; **24**: 502–11. doi: http://dx.doi.org/10.1007/s00330-013-3048-y